



# Miniaturized diplexer with wide-stopband based on half-mode SIW\*

Ziyu ZHOU, Gang DONG<sup>‡</sup>, Xinqing LEI, Zhangming ZHU

*School of Microelectronics, Xidian University, Xi'an 710071, China*

E-mail: 22111110508@stu.xidian.edu.cn; gdong@xidian.edu.cn; 23111110115@stu.xidian.edu.cn; zmyh@263.net

Received Oct. 20, 2024; Revision accepted Jan. 24, 2025; Crosschecked

**Abstract:** A miniaturized diplexer with wide-stopband based on half-mode substrate integrated waveguide (HM-SIW) is proposed. The diplexer combines dual-mode resonator (DMR) with single-mode resonators (SMRs). The employment of HMSIW technology breaks through the limitations of SMRs on miniaturization, while effectively addressing the limitation on wide-stopband performance that is typically encountered with the TE<sub>202</sub> mode in the SMRs. A second-order prototype, centered at 10.34 GHz and 13.9 GHz, has been designed and fabricated, utilizing a TE<sub>101</sub>/TE<sub>301</sub> DMR. The measured out-of-band rejection is better than 20 dB with a frequency of up to 2.16  $f_1$ . Meanwhile, the size of the diplexer is reduced to 1.363  $\lambda_g^2$ .

**Key words:** Diplexer; Substrate integrated waveguide; Miniaturization; Half-mode; Wide-stopband; Intrinsic mode suppression technique

<https://doi.org/10.1631/FITEE.2400944>

**CLC number:** TN

## 1 Introduction

As a special type of filter, diplexers separate the transmission and reception channels of a common antenna. Due to the significant impact on wireless communication systems, the trend in diplexer design focuses on wide-stopband performance, high isolation, low insertion loss, and miniaturization (Bavandpour et al., 2021; Roshani et al., 2023). Substrate integrated waveguide (SIW) technology has become an effective solution for diplexer designs as it provides high Q and electromagnetic interference shielding while significantly reducing size.

In a conventional design, T-junctions are used in diplexers to separate two passbands (Sirici et al., 2015). Many studies aim to minimize the circuit size by eliminating T-junctions. A compact

diplexer is proposed (Cheng et al., 2013), using multiple dual-mode resonator (DMR) connections, which cannot control the bandwidth of two channels separately. Another approach integrates DMR and single-mode resonators (SMRs) within the diplexer to independently control the bandwidth of each passband, establishing a classic topology (Zhou et al., 2018a). However, this topology still incorporates multiple SMRs, which occupy a significant amount of space and hinder further miniaturization. Alternative miniaturization methods have been proposed, such as multi-layer stacking technology (Iqbal et al., 2019), half-mode substrate integrated waveguide (HMSIW) (Zhou and Wu, 2021) and folded SIW (Sieganschin et al., 2021). Nevertheless, both multi-layer technology, and folded SIW increase the design complexity and manufacturing costs.

The stopband characteristic is also one of the key performances of diplexers as the wide-stopband can effectively reduce the external or internal signal interference. However, designing compact SIW diplexers with wide-stopband remains a challenge.

<sup>‡</sup> Corresponding author

\* Project supported by the National Natural Science Foundation of China (Nos. U23A20291 and 62021004) and the National Key Research and Development Program of China (No. 2023YFF0616600)

© Zhejiang University Press 2025

Building on the topology that combines DMR and SMRs, various techniques have been implemented to achieve wide-stopband SIW diplexers without T-junctions, such as the harmonic staggered technique (Zhou et al., 2020), orthogonal transmission (Xie et al., 2020), and center-coupled windows (Ma et al., 2023). However, in these studies, since the  $TE_{202}$  mode in the SMRs is not completely suppressed, the boundary of the stopband is limited to around  $2f_1$ .

In this study, a compact and wide-stopband SIW diplexer is proposed, based on HMSIW technology. Utilizing half-mode substrate integrated rectangular cavities (HMSIRC)s as both DMR and SMRs overcomes the limitations of SMRs on the miniaturization and wide-stopband performance. The  $TE_{202}$  mode is effectively eliminated from SMRs as certain even modes in HMSIRC are not excited due to magnetic walls in the symmetry plane (Lai et al., 2009). The  $TE_{102}$  mode is suppressed, elevating  $TE_{301}$  as the first unsuppressed mode in SMRs. Therefore, the diplexer can obtain a wider stopband only through second-order resonance. The usage of HMSIRCs, coupled with a reduced number of resonators, further minimizes the circuit size. A second-order prototype based on  $TE_{101}/TE_{301}$  DMR is designed and fabricated, covering a wide range of frequency ratios. Measurements show that the prototype exhibits excellent stopband performance with a small size.

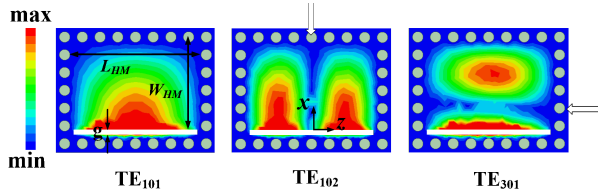


Fig. 1 Electric field magnitude distributions of  $TE_{101}$ ,  $TE_{102}$ , and  $TE_{301}$  modes in an HMSIRC. HMSIRC, half-mode substrate-integrated rectangular cavity.

## 2 Realization method of dual-band and wide-stopband

In the proposed diplexer, the first two modes in the DMR and the first mode in the SMRs form two passbands. To achieve dual-band and wide-stopband, the higher-order mode characteristics of HMSIRC are analyzed. Substrate integrated rectangular cavity (SIRC), the equivalent structure of HMSIRC, has dimensions resonant frequencies of the

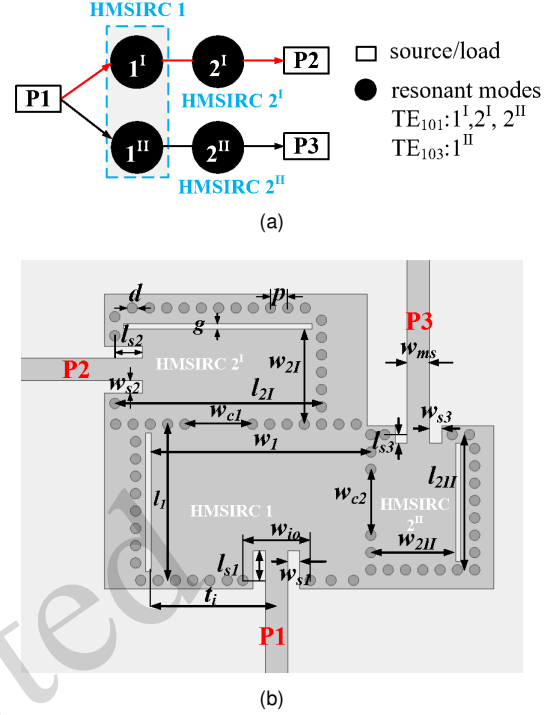


Fig. 2 Proposed SIW diplexer based on HMSIRC. (a) Coupling topology and (b) Geometric configuration. HMSIRC, half-mode substrate-integrated rectangular cavities; SIW, substrate-integrated waveguide.

first three modes, we can obtain  $f_1 = f_{TE_{101}}$ . Normalized frequency ratios  $k_{m0q}$  are used to analyze higher-order distributions, which can be deduced using Eq. (1) (Zhou et al., 2017).

$$k_{m0q} = \frac{f_{TE_{m0q}}}{f_{TE_{101}}} = \sqrt{q^2 + \frac{m^2 - q^2}{1 + (W/L)^2}} \quad (1)$$

denoted by  $W$  and  $L$  in the  $x$ - and  $z$ -axis directions ( $W \geq L$ ). If we define  $f_1$ ,  $f_2$ , and  $f_3$  as the where  $m$  and  $q$  are the mode indices along the  $x$ - and  $z$ -axis directions, respectively. Considering the removed modes  $TE_{201}$  and  $TE_{202}$ , the higher-order mode distributions in HMSIRC can be divided into three main cases based on the  $W/L$  ratio, as shown in Table 1. From Table 1, we can deduce that the realizable range of  $f_2/f_1$  is  $[1.1.784]$  when the second mode in HMSIRC is  $TE_{301}$ . Therefore, DMR is designed with  $f_1 = f_{TE_{101}}$  and  $f_2 = f_{TE_{301}}$  to achieve a wide range of realizable frequency ratios.

To achieve wide-stopband, the third mode in DMR and the second mode in SMRs should be suppressed by strategically positioning the internal coupling windows within the regions of the weakest electric field for each respective mode. The electric field

magnitude distributions of the  $TE_{101}$ ,  $TE_{102}$ , and  $TE_{301}$  modes in an HMSIRC and their suppression positions are shown in Fig. 1. The internal coupling window for the HMSIRC should be set at half of the common post-wall along the  $z$ -axis if the  $TE_{102}$  mode is to be suppressed. If the  $TE_{301}$  mode is to be suppressed, the internal coupling window should be set at one-third of the common post-wall along the  $x$ -axis. From Table 1, it can be concluded that the values of  $f_2/f_1$  and  $f_3/f_1$  increase as  $W/L$  decreases. The  $W/L$  ratio of SMRs is designed to be close to 1 to stagger the higher order modes in DMR and SMRs. Therefore, the second mode in SMRs is the  $TE_{102}$  mode. Due to the inhibition of the  $TE_{102}$  mode in SMRs, the first unsuppressed mode in SMRs is the  $TE_{301}$  mode, which specifies the stopband boundary of the diplexer. Consequently, the stopband of the proposed diplexer can be extended to  $2.236 f_1$  at most. For whole mode SMRs with the same  $W/L$  ratio,  $TE_{202}$  is the first unsuppressed mode, thus achieving a maximum stopband of  $2 f_1$  for the diplexer.

**Table 1 Cases of higher order mode characteristics of HMSIRC with different  $W/L$ .**

Cases	Case 1	Case 2	Case 3
$W/L$	[1,1.633]	[1.633,2.828]	[2.828, $+\infty$ ]
1 <sup>st</sup> mode	$TE_{101}$	$TE_{101}$	$TE_{101}$
2 <sup>nd</sup> mode	$TE_{102}$	$TE_{301}$	$TE_{301}$
3 <sup>rd</sup> mode	$TE_{301}$	$TE_{102}$	$TE_{501}$
$f_2/f_1$	[1.581,1.784]	[1.374,1.784]	(1,1.374]
$f_3/f_1$	[1.784,2.236]	[1.172,1.837]	(1,1.914]

### 3 Synthesis and design of wide-stopband diplexer based on HMSIW

#### 3.1 Coupling topology

Fig. 2a depicts the coupling topology of the second-order prototype. HMSIRC 1 operates with the  $TE_{101}$  resonance at  $f_1$  and the  $TE_{301}$  resonance at  $f_2$ , while HMSIRC 2<sup>I</sup> and 2<sup>II</sup> operate with  $TE_{101}$  resonances at  $f_1$  and  $f_2$ , respectively. The configuration of the proposed diplexer is shown in Fig.2b. It can be seen that input port 1 is set to offset  $t_i$  to control the external couplings of the two modes for flexible control of the dual bandwidth. The internal coupling window between HMSIRC 1 and 2<sup>I</sup> rejects the  $TE_{102}$  mode in HMSIRC 2<sup>I</sup>. Additionally, the

internal coupling window between HMSIRC 1 and 2<sup>II</sup> rejects the  $TE_{102}$  mode in HMSIRC 2<sup>II</sup>.

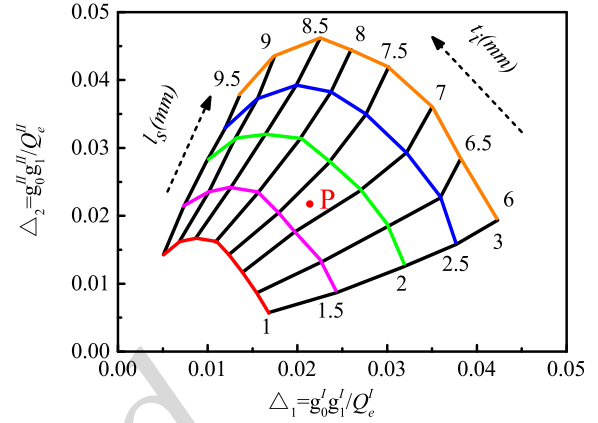


**Fig. 3 FBW design graph for the SIW diplexer. Dimensions in millimeter:  $w_{ms} = 1.29$ ,  $w_s = 0.7$ ,  $w_{i0} = 3.9$ ,  $w_1 = 9$ , and  $l_1 = 12.7$ . FBW, fractional bandwidth.**

#### 3.2 Design parameters and FBW design graph

This second-order diplexer is synthesized according to the conventional Chebyshev prototype filter with a return loss (RL) around 20 dB. The element values of the corresponding low-pass prototype filter can be found as  $g_0^{I,II} = 1$ ,  $g_1^{I,II} = 0.6648$ ,  $g_2^{I,II} = 0.5445$ ,  $g_3^{I,II} = 1.2210$  (Hong and Lancaster, 2004). The diplexer is designed and fabricated on the Rogers RT/Duroid 3003 substrate (dielectric constant  $\epsilon_r = 3$ , thickness  $h = 0.508$  mm, and loss tangent  $\tan\delta = 0.001$ ). The diameter ( $d$ ) of metallized via-holes and the distance ( $p$ ) between the adjacent via-holes in the cavity are 0.6 mm and 1 mm, respectively. The physical sizes of the HMSIRCs can be calculated using Eqs (2)–(4) (Zhou et al., 2018b).

$$W_{HMSIRC} = W_{SIRC}/2 - \Delta W \quad (2)$$

$$L_{HMSIRC} = L_{SIRC} \quad (3)$$

$$\frac{\Delta W}{h} = \left( 0.05 + \frac{0.03}{\epsilon_r} \right) \times \ln \left( 0.79 \frac{(W/2)^2}{h^3} + \frac{104(W/2) - 261}{h^2} + \frac{38}{h} + 2.77 \right) \quad (4)$$

where  $W_{HMSIRC}$  and  $L_{HMSIRC}$  represent the width and length of an HMSIRC, while  $W_{SIRC}$  and  $L_{SIRC}$

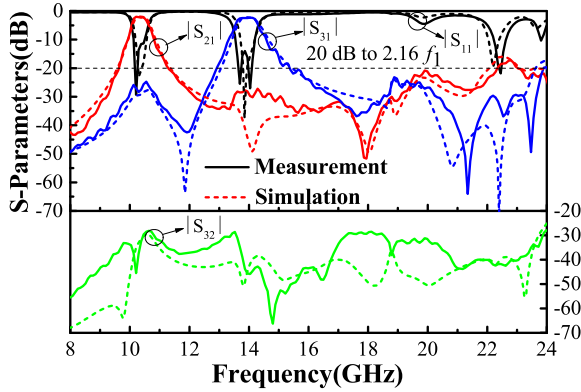


Fig. 4 Comparison between the simulated and measured results of the proposed diplexer.

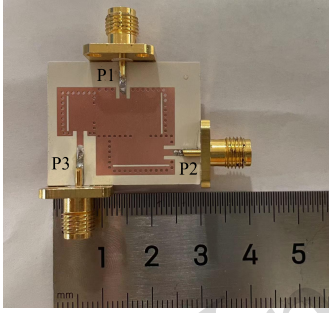


Fig. 5 The photograph of the fabricated prototype.

represent the width and length of the corresponding SIRC, respectively.  $\Delta W$  describes the effect of fringing fields on the open boundary of HMSIRC (Zhou et al., 2018b). In addition,  $\epsilon_r$  is the relative permittivity. The initial size of HMSIRC 1 can be calculated with  $f_1 = f_{TE101} = 10.34$  GHz and  $f_2 = f_{TE301} = 13.9$  GHz. The fractional bandwidths (FBWs) of the lower and upper channel filters ( $\Delta_1$  and  $\Delta_2$ ) can be obtained using Eq. (5):

$$\begin{aligned} \Delta_1 &= g_0^I g_1^I / Q_e^I = M_{12}^I \sqrt{g_1^I g_2^I} \\ \Delta_2 &= g_0^{II} g_1^{II} / Q_e^{II} = M_{12}^{II} \sqrt{g_1^{II} g_2^{II}} \end{aligned} \quad (5)$$

where  $Q_e^{I,II}$  are the external quality factors, and can be easily calculated based on the Eq. (6):

$$Q_e^{I,II} = \frac{2\pi f_0^{I,II} \cdot \tau_{S11}(f_0^{I,II})}{4} \quad (6)$$

while  $M_{12}^{I,II}$  are the internal coupling coefficients in the two channels, which can easily be extracted with Eq. (7)

$$M_{12}^{I,II} = \left( \frac{f_H^2 - f_L^2}{f_H^2 + f_L^2} \right)^{I,II} \quad (7)$$

where  $f_0^{I,II}$  are resonant frequencies of TE<sub>101</sub> and TE<sub>201</sub> modes, while  $\tau_{S11}(f_0^{I,II})$  are group delays of  $S_{11}$  at  $f_0^{I,II}$ , respectively. According to Eq. (5), if the diplexer is established with  $\Delta_1 = 2.14\%$  and  $\Delta_2 = 2.15\%$ , the theoretical  $Q_e$  of the two passbands can be determined as  $Q_e^I = 31.06$  and  $Q_e^{II} = 30.92$ . Then the corresponding coupling matrices of the two channels can be obtained according to Eq. (5):

$$[M^I] = \begin{bmatrix} 0 & 0.0355 \\ 0.0355 & 0 \end{bmatrix} \quad (8)$$

$$[M^{II}] = \begin{bmatrix} 0 & 0.0375 \\ 0.0375 & 0 \end{bmatrix} \quad (9)$$

Hence, with the given design bandwidths of the lower and upper channel filters, we can separately determine the size of the coupling windows and the coupling degree of the output port for filters of each channel. Meanwhile, the dimension of the common input port P1 needs to be designed according to the bandwidth requirements of two channels. Fig. 3 shows the available FBWs of the two channels against the offset  $t_i$  and the length of the input port  $l_{s1}$  with fixed  $w_{ms} = 1.29$  mm,  $w_s = 0.7$  mm, and  $w_{i0} = 3.9$  mm. According to the FBW design graph, when the diplexer is established with  $\Delta_1 = 2.14\%$  and  $\Delta_2 = 2.15\%$ , the parameters of the input port are displayed by point P as  $t_i = 7.25$  mm and  $l_{s1} = 1.7$  mm.

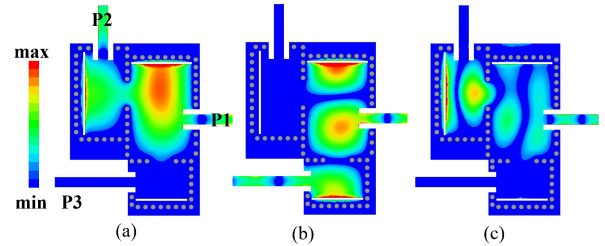


Fig. 6 Electric field magnitude distributions in the diplexer at (a) 10.34 GHz, (b) 13.9 GHz, and (c) 22.5 GHz.

### 3.3 Electric field distributions and experimental results

The S-parameters of the diplexer obtained by simulation and measurement are displayed in Fig. 4. The detailed dimensions of the intended diplexer are listed in Table 2. The measurement results of the diplexer are roughly consistent with the simulation results. The center frequencies of the two channels are 10.34 GHz and 13.9 GHz, with 3 dB bandwidths

Table 2 Parameter list

Parameters	$w_{ms}$	$w_{s1}$	$w_{s2}$	$w_{s3}$	$w_{i0}$	$w_1$	$l_1$	$w_{2I}$	$l_{2I}$
Values(mm)	1.29	0.7	0.7	0.7	3.9	9	12.7	5.5	11.95
Parameters	$w_{2II}$	$l_{2II}$	$t_i$	$l_{s1}$	$l_{s2}$	$l_{s3}$	$w_{c1}$	$w_{c2}$	
Values(mm)	4.9	7.8	7.25	1.7	1.6	0.5	3.9	3.8	

Table 3 Comparisons with other reported SIW diplexers

Ref.	Order	$f_1/f_2$ (GHz)	3-dB/ FBW(%)	Isolation(dB)	Rejection/ stopband	IL (dB)	Size( $\lambda_g^2$ )
(Zhou et al., 2018a)	3/3	12/14	4.9/5.65	27	20 dB/1.45 $f_1$	1.34/1.41	2.77
(Iqbal et al., 2019)	2/2	10.5/13.5	3.71/1.7	42	20 dB/2 $f_1$	0.8/1.35	2.78
(Zhou and Wu, 2021)	3/3	3.5/5	4/3.2	45.8	20 dB/1.7 $f_1$	2.77/2.55	1.62
	4/4	3.5/5.5	3.43/2.55	27.6	20 dB/2.05 $f_1$	3.41/3.4	1.136
(Xie et al., 2020)	2/2	10/12.25	4/3.2	20	24 dB/1.79 $f_1$	2.05/1.65	2.34
	2/2	8/12	3.43/2.55	20	20 dB/2.05 $f_1$	1.84/2.88	1.54
(Ma et al., 2023)	3/3	12/14	2.04/2.44	22	20 dB/1.32 $f_1$	2.51/2.19	3.47
	3/3	12/14	3.73/3.99	47	20 dB/2.02 $f_1$	1.39/1.37	3.62
(Liu et al., 2023)	4/4	34.95/36.44	1.73/ 1.39	28.9	20 dB/ 2.37 $f_1$	4.24/5.1	12.6
This work	2/2	10.34/13.9	5.7/5.83	28.1	20 dB/2.16 $f_1$	2.03/2.33	1.363

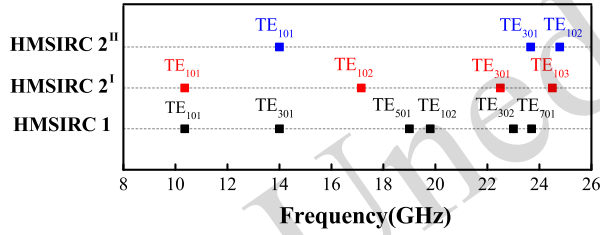


Fig. 7 Frequency spectrum of initial resonances for the HMSIRCs in the proposed diplexer.

of 590 MHz and 810 MHz, respectively. The minimum insertion losses in the two channels are 2.03 dB and 2.33 dB, respectively. The isolation exceeds 28.1 dB. The measured stopband extends to  $2.16 f_1$  with a rejection of more than 20 dB. Fig. 5 shows the photograph of the fabricated prototype. The dimensions of the diplexer are  $22.5 \text{ mm} \times 17 \text{ mm}$  ( $1.343 \lambda_g \times 1.015 \lambda_g$ ).  $\lambda_g$  is the guided wavelength in dielectric substrate at  $f_1$ . Figs. 6a and 6b show the electric field distributions in the diplexer at 10.34 GHz ( $f_1$ ) and 13.9 GHz ( $f_2$ ), respectively. It proves that the lower channel is composed of  $TE_{101}$  mode in HMSIRCs 1 and  $2^I$ , while the upper channel is composed of the  $TE_{301}$  mode in HMSIRC 1 and the  $TE_{101}$  mode in HMSIRC  $2^{II}$ . Fig. 6c illustrates the electric field distributions in the diplexer at the stopband edge (22.4 GHz). The  $TE_{301}$  mode in HMSIRC  $2^I$  excites the HMSIRC 1, resulting in the  $|S_{21}|$  peak at 22.4 GHz.

## 4 Discussions and comparisons

Fig. 7 illustrates the resonant mode ss of the three HMSIRCs, revealing a staggered higher-order mode distribution in the frequency spectrum. Comparing Fig. 4 with Fig. 7, we can infer that the peak of  $|S_{21}|$  at 22.5 GHz in Fig. 4 is caused by the  $TE_{301}$  mode in HMSIRC  $2^I$ . Additionally, the  $|S_{21}|$  peak of the diplexer at 20 GHz is caused by the  $TE_{501}$  and  $TE_{102}$  modes in HMSIRC 1. Despite HMSIRC  $2^I$  showing a  $TE_{102}$  mode response at 17.1 GHz,  $|S_{21}|$  does not exhibit a significant peak at this frequency due to the suppression of the coupling window. Therefore, the stopband boundary of the proposed diplexer mainly depends on the first unsuppressed mode in HMSIRC  $2^I$ . Table 3 shows comparisons between the proposed diplexer and other SIW diplexers. Compared to the designs in the studies by Zhou et al. (2018a), Iqbal et al. (2019), Zhou and Wu (2021), Xie et al. (2020) and Ma et al. (2023), the diplexer we proposed has a wider stopband. In the study by Liu et al. (2023), various techniques were used to design a wide-stopband diplexer, yet the circuit area remains large. Our proposed diplexer exhibits superior stopband performance and maintains compactness.

## 5 Conclusions

A planar SIW diplexer, based on HMSIW technology, is proposed featuring a wide-stopband and a



compact circuit size. Utilizing HMSIRCs in place of whole-mode SIRCs as resonators not only broadens the stopband of the diplexer but also minimizes the circuit area. A second-order prototype centered at 10.34 and 13.9 GHz is fabricated and measured, extending the stopband up to  $2.16 f_1$  with better than 20 dB rejection level.

### Contributors

Ziyu ZHOU designed the research and wrote the paper. Xinqing LEI helped organize the paper. Gang DONG and Zhangming ZHU revised and finalized the paper.

### Conflict of interest

All the authors declare that they have no conflict of interest.

### References

- Bavandpour SK, Roshani S, Pirasteh A, et al., 2021. A compact lowpass-dual bandpass diplexer with high output ports isolation. *AEU-Int J Electr Commun*, 135:153748. <https://doi.org/10.1016/j.aeue.2021.153748>
- Cheng F, Lin XQ, Song KJ, et al., 2013. Compact diplexer with high isolation using the dual-mode substrate integrated waveguide resonator. *IEEE Microw Wirel Compon Lett*, 23(9):459-461. <https://doi.org/10.1109/LMWC.2013.2274036>
- Hong JSG, Lancaster MJ, 2004. *Microstrip filters for RF/microwave applications*. John Wiley & Sons, New York, USA.
- Iqbal A, Tiang JJ, Lee CK, et al., 2019. Tunable substrate integrated waveguide diplexer with high isolation and wide stopband. *IEEE Microw Wirel Compon Lett*, 29(7):456-458. <https://doi.org/10.1109/LMWC.2019.2916609>
- Lai QH, Fumeaux C, Hong W, et al., 2009. Characterization of the propagation properties of the half-mode substrate integrated waveguide. *IEEE Trans Microw Theory Tech*, 57(8):1996-2004. <https://doi.org/10.1109/TMTT.2009.2025429>
- Liu N, Fan CH, Liu XX, et al., 2023. Wide-stopband diplexer with small frequency ratio based on siw dual-mode resonators for millimeter-wave applications. *IEEE Trans Compon Packag Manuf Technol*, 13(2):284-287. <https://doi.org/10.1109/TCPMT.2023.3243204>
- Ma DD, Zhou K, Xie HW, et al., 2023. Compact or wide-stopband siw diplexers with high intrinsic isolations based on orthogonal dual modes. *IEEE Trans Circ Syst II: Express Briefs*, 70(1):71-75. <https://doi.org/10.1109/TCSII.2022.3208663>
- Roshani S, Yahya SI, Mezaal YS, et al., 2023. Design of a compact quad-channel microstrip diplexer for 1 and s band applications. *Micromachines*, 14(3):553. <https://doi.org/10.3390/mi14030553>
- Sieganschin A, Tegowski B, Jaschke T, et al., 2021. Compact diplexers with folded circular siw cavity filters. *IEEE Trans Microw Theory Tech*, 69(1):111-118. <https://doi.org/10.1109/TMTT.2020.3039545>
- Sirci S, Martínez JD, Vague J, et al., 2015. Substrate integrated waveguide diplexer based on circular triplet combline filters. *IEEE Microw Wirel Compon Lett*, 25(7):430-432. <https://doi.org/10.1109/LMWC.2015.2427516>
- Xie HW, Zhou K, Zhou CX, et al., 2020. Compact siw diplexers and dual-band bandpass filter with wide-stopband performances. *IEEE Trans Circ Syst II: Express Briefs*, 67(12):2933-2937. <https://doi.org/10.1109/TCSII.2020.2992059>
- Zhou K, Wu K, 2021. Miniaturized diplexers with large frequency ratios based on common half-mode dual-mode siw junction-cavities. *IEEE Trans Microw Theory Tech*, 69(12):5343-5350. <https://doi.org/10.1109/TMTT.2021.3113012>
- Zhou K, Zhou CX, Wu W, 2017. Resonance characteristics of substrate-integrated rectangular cavity and their applications to dual-band and wide-stopband bandpass filters design. *IEEE Trans Microw Theory Tech*, 65(5):1511-1524. <https://doi.org/10.1109/TMTT.2016.2645156>
- Zhou K, Zhou CX, Wu W, 2018a. Compact siw diplexer with flexibly allocated bandwidths using common dual-mode cavities. *IEEE Microw Wirel Compon Lett*, 28(4):317-319. <https://doi.org/10.1109/LMWC.2018.2805881>
- Zhou K, Zhou CX, Wu W, 2018b. Dual-mode characteristics of half-mode siw rectangular cavity and applications to dual-band filters with widely separated passbands. *IEEE Trans Microw Theory Tech*, 66(11):4820-4829. <https://doi.org/10.1109/TMTT.2018.2865557>
- Zhou K, Zhou CX, Wu W, 2020. Compact planar substrate-integrated waveguide diplexers with wide-stopband characteristics. *Int J RF Microw Comput-Aided Eng*, 30(6):e22179. <https://doi.org/10.1002/mmce.22179>